HAL
open science

On the Use of Quantum Thermal Bath in Unimolecular Fragmentation Simulation

Riccardo Spezia, Hichem Dammak

To cite this version:

Riccardo Spezia, Hichem Dammak. On the Use of Quantum Thermal Bath in Unimolecular Fragmentation Simulation. Journal of Physical Chemistry A, 2019, 123 (40), pp.8542-8551. 10.1021/acs.jpca.9b06795 . hal-02309300

HAL Id: hal-02309300

https://hal.science/hal-02309300v1

Submitted on 30 Oct 2019

HAL is a multi-disciplinary open access archive for the deposit and dissemination of scientific research documents, whether they are published or not. The documents may come from teaching and research institutions in France or abroad, or from public or private research centers.

L'archive ouverte pluridisciplinaire **HAL**, est destinée au dépôt et à la diffusion de documents scientifiques de niveau recherche, publiés ou non, émanant des établissements d'enseignement et de recherche français ou étrangers, des laboratoires publics ou privés.

On the Use of Quantum Thermal Bath in Unimolecular Fragmentation Simulations

Riccardo Spezia[*,†] and Hichem Dammak[‡]

†*Laboratoire de Chimie Théorique, Sorbonne Université and CNRS, F-75005 Paris, France*

‡*Laboratoire Structures Propriétés et Modélisation des Solides, CentraleSupélec, CNRS, Université Paris-Saclay, F 91190 Gif-sur-Yvette, France*

E-mail: riccardo.spezia@sorbonne-universite.fr

Abstract

In the present work we have investigated the possibility of using the Quantum Thermal Bath (QTB) method in molecular simulations of unimolecular dissociation processes. Notably, QTB is aimed in introducing nuclear quantum effects with a computational time which is basically the same as in newtonian simulations. At this end, we have considered the model fragmentation of CH_4 for which an analytical function is present in the literature. Moreover, based on the same model, a microcanonical algorithm, which monitors the zero-point energy of products, and eventually modifies trajectories, was recently proposed. We have thus compared classical and quantum rate constant with these different models. QTB seems to correctly reproduce some quantum features, in particular the difference between classical and quantum activation energies, making it a promising method to study, with molecular simulations, unimolecular fragmentation of much complex systems. The role of QTB thermostat on rotational degrees of freedom is also analyzed and discussed.

September 9, 2019

Introduction

Unimolecular dissociation represents one of the elementary chemical process which is involved in a series of phenomena, like e.g. collisional activation fragmentation or laser induced reactivity.[1] The kinetics of this process is described by a simple exponential decay of the initial microcanonical ensemble,[2] $N(0)$:

$$\frac{N(t)}{N(0)} = e^{-kt} = e^{-t/\tau} \tag{1}$$

where k is the unimolecular rate constant and τ the lifetime. The well-known Rice-Ramsperger-Kassel-Marcus (RRKM) statistical theory is often employed to describe this

process,[1,3,4] also called Quasi-Equilibrium theory (QET).[5–7] In this framework, the initial ensemble decays with a single exponential behavior and the rate constant, k, is the RRKM rate constant. If information on reactants and transition states are available, it is possible to obtain both $k(E)$ and $k(T)$ by means of analytical models. Analytical theories are surely very powerful, but have limited applications: one has to determine partition functions (or density of states) of reactants and transition states and all the possible pathways should be known in advance. Harmonic approximation is often employed: anharmonicity can be added but this becomes almost impossible for relatively large molecules. Explicit simulations have been used and developed to directly obtain unimolecular fragmentation dynamics and products.[8–11] At this aim, chemical dynamics simulations were used with different ways of energizing the fragmenting molecule:[12] (i) giving an excess of internal energy, (ii) by explicit collision with an inert gas. For example, it was possible to understand products structures and reaction mechanisms in collision induced dissociation (CID) of several systems, from small organic molecules,[13–15] to biological molecules like peptides[16–20] or sugars.[21,22]

In addition to information on fragmentation products and mechanisms, chemical dynamics can be used to obtain kinetic informations on unimolecular dissociation. In particular, from time decay of the initial population it is possible to obtain rate constants[9,10,16,18] and in some case threshold energies, via a correspondence between classical microcanonical RRKM expression (called also RRK theory) and temperature dependence of the rate constant which assumes an Arrhenius-like form. These dynamics are purely newtonian, and thus rate constants are classical and anharmonic – the anharmonicity comes directly since the simulations are done on-the-fly on the full potential energy surface which is not harmonic. Nuclear quantum effects (NQE) are not considered and this can impact the simulations outcome for (at least) three aspects: (i) the rate constant is classical; (ii) the activation or threshold energies will not consider zero-point energy (ZPE) difference between reactant and transition state (and/or products); (iii) tunneling is not considered. Furthermore, there can be in principle a difference between classical and quantum dynamics in reaction product ratio for the

fragmentation of a complex molecule, with an effect on product abundances and even on appearance of some of them.

In endothermic unimolecular dissociation an important NQE is related to the ZPE of the products. In classical simulations, in fact, it is possible to form products with vibrational energy smaller than their ZPE, which is not allowed in quantum dynamics.

To recover at least some of these NQE, a number of methodologies were proposed in last years. Methods based on path integral molecular dynamics, like ring polymer MD (RPMD)[23] or centroid MD (CMD)[24] can provide ZPE conservation.[25,26] They are based on path integral theory[27,28] and thus well designed for thermodynamic properties.[29] They are also used for dynamical quantities but they must be carefully handled.[30] Computationally, they increase the simulation time by a factor P with respect to a classical trajectory, where P is the number of beads which represents each particle in the path-integral formalism.

Semi-classical methods[31] can overcome most of the problems related to incorrect treatment of NQE in trajectories, like was shown recently[32] in the case of Herman-Kluk propagator,[33] but they need a huge statistics to converge and are rarely applicable to systems with more than three degrees of freedom. More in general, in last years, a number of methods were proposed to specifically avoid ZPE leakage, often based on the knowledge of normal modes and projection of actual positions and momenta on internal coordinates.[34–37]

Recently, Dammak and co-workers have proposed a method called Quantum Thermal Bath (QTB)[38] which can recover some NQE of vibrational motion. This method was mainly tested for condensed phase systems.[39–44] It is based on a Langevin-dynamics formalism with a colored noise (which keeps quantum vibrational properties) and computationally it has almost the same cost as newtonian dynamics. Furthermore, it can be applied to molecular dynamics propagation without any need of specific knowledge of ZPE or instantaneous normal modes. Being promising for its use in a range of problems, its applicability to model chemical reactions, and in particular unimolecular dissociations, was never extensively investigated. Proton transfer was studied in solids[43,44] or to better describe spectroscopy of

isolated molecules.[42]

In the present work, we study the case of a model unimolecular reaction, notably the homolytic dehydrogenation of CH_4 in the gas phase. Recently, the same system was studied by Paul and Hase[45] by comparing purely classical fragmentation with trajectories in which the ZPE energy of the forming products was checked and trajectories modified if they do not have enough ZPE. Following the spirit of original Miller-Hase-Darling method[46] for constraining ZPE in non-reactive systems, in the present case if a trajectory is leaving the reactant basin without enough ZPE in the product (here CH_3) it is sent back to reactants and "another chance" to react with the correct ZPE is given. We have thus used the same fragmentation model to understand how QTB can include NQE in unimolecular reactivity. One of the main questions addressed here is whether QTB activation energy can reflect the difference in ZPE between reactants and products, which modifies the barrier with respect to classical dynamics. Furthermore, we have investigated how, from microcanonical simulations at different energies, the Paul and Hase correction to trajectories impacts the energy evolution of rate constants and thus of activation energies. Finally, using well-known relationship connecting $k(E)$ and $k(T)$ it was possible to compare the different approaches on the same reaction.

Models and Methods

Model for $CH_4 \rightarrow \cdot CH_3 + \cdot H$ Dissociation

We have employed the well-studied Duchovic-Hase-Schelegel (DHS) model[47] for CH_4 homolytic dehydrogenation with later modifications.[48,49] It is composed by a set of Morse functions for the C–H bonds plus additional torsional potential to keep the tetrahedral structure. Details of the model are given in the Supporting Information. Note that another model for CH_4 is present in the literature,[50,51] but here we used the same modified-DHS model employed by Paul and Hase in order to be comparable with this recent study.[45] The

aim of the present work is merely to understand QTB performances in unimolecular dissociation, in order to eventually use it for other more complex systems. Furthermore, the DHS model was built from *ab initio* calculations and it does not implicitly incorporate any NQE, opposed to force fields based on empirical data. The DHS model was shown to be able to correctly reproduce thermal rate constants for $\cdot H + \cdot CH_3$ recombination[48] and (using a slightly DHS model) thermal rate coefficient for $CH_4 + Ar \rightarrow \cdot CH_3 + \cdot H + Ar$ reaction using quasi-classical trajectories imposing ZPE conditions on products.[52]

Within this potential, the ZPE of the reactant, CH_4, is 29.17 kcal/mol, and that of the CH_3 product is 18.60 kcal/mol. The classical fragmentation barrier is 109.46 kcal/mol, while, taking into account ZPE of reactant and products, the barrier is expected to drop down to 98.89 kcal/mol.

This model was recently used by Paul and Hase to investigate the microcanonical dissociation kinetics using a purely classical dynamics with a new algorithm which keeps the system back to reactant if the products (CH_3) are obtained without enough ZPE.[45] In this work, the C–H distance of 6 Å was fixed as the value to define when a dissociation is done (irreversibly). This value was chosen as in Ref.[45] such that we can directly compare results for both canonical and microcanonical simulations.

Within this model, and the energies employed here, the unimolecular fragmentation reaction allowed to occur is:

$$CH^*_{4(g)} \rightarrow \cdot CH_{3(g)} + \cdot H_{(g)} \tag{2}$$

Using the harmonic frequencies of the DHS model for CH_4, the average classical, E^{cl}, and quantum, E^q, vibrational energies as a function of the temperature, T, can be calculated from the classical statistical mechanics and Bose-Einstein statistics, respectively:

$$\langle E^{cl} \rangle = N k_B T \tag{3}$$

$$\langle E^{q} \rangle = \sum_{i}^{N} \hbar\omega_i \left(\frac{1}{2} + \frac{1}{e^{\beta\hbar\omega_i} - 1} \right) \tag{4}$$

where N is the number of vibrational frequencies, k_B is the Boltzmann constant, ω_i are the vibrational angular frequencies, $\hbar$ is the reduced Planck's constant and $\beta = 1/k_B T$. The temperature dependence of classical and quantum average vibrational energies for the present CH_4 model is reported in Figure 1.

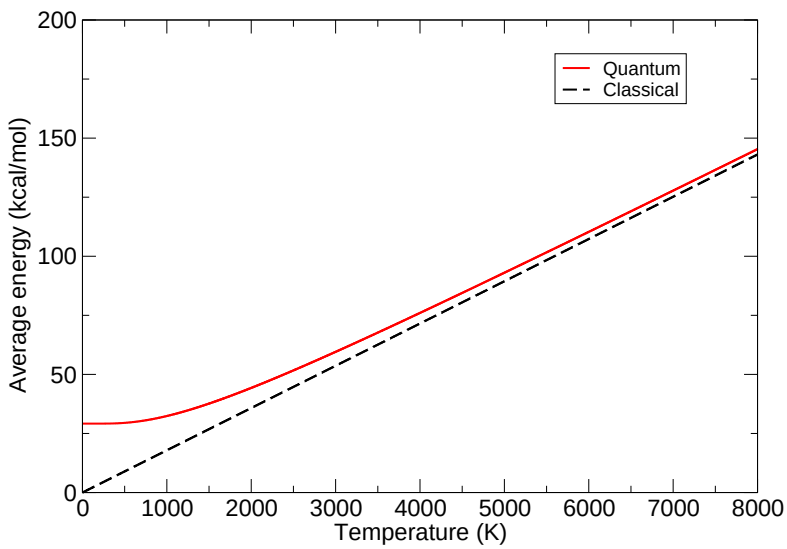

Figure 1: Quantum versus classical average vibrational energy of the CH_4 model employed as a function of temperature.

Quantum Thermal Bath Simulations

Molecular dynamics simulations were done using the Quantum Thermal Bath (QTB) method to take into account NQE.[38] The Langevin formal structure of equations of motion is used

$$m_i \ddot{q}_{i,\alpha} = -\frac{\partial V}{\partial q_{i,\alpha}} - m_i \gamma \dot{q}_{i,\alpha} + R_{i,\alpha}(t) \tag{5}$$

where i runs on the atoms, $\alpha = x, y, z$, m_i is the mass, $\dot{q}_{i,\alpha}$ and $\ddot{q}_{i,\alpha}$ are the first and second time derivatives of the positions, V the interaction potential between the nuclei (here the modified DHS described previously), γ an effective frictional coefficient and $R_{i,\alpha}(t)$ is the random force which in QTB method is set in order to have the correct spectral density, I_R, following the Wiener-Khinchin theorem

$$\langle R_{i,\alpha}(t) R_{i,\alpha}(t+\tau) \rangle = \int_{-\infty}^{+\infty} I_{R_i}(|\omega|) e^{-i\omega\tau} \frac{d\omega}{2\pi} \tag{6}$$

where I_{R_i} obeys to the fluctuation-dissipation theorem for quantum systems:[53]

$$I_{R_i}(\omega) = 2 m_i \gamma \hbar \omega \left[\frac{1}{2} + \frac{1}{\exp(\beta \hbar \omega) - 1} \right] \tag{7}$$

The random force was generated as reported previously[54,55] before each simulation and then equations of motion are integrated with modified velocity Verlet algorithm with a time step of 0.1 fs. Different γ values were employed and results studied as a function of this parameter.

Six temperatures were considered in fragmentation simulations: 3000, 3500, 4000, 4500, 5000 and 5500 K. For each set of simulations, 500 trajectories were done, with variable length (between 5 ps and 1 ns) as a function of temperature. These time-lengths were chosen in order to have almost 100 % of reactive trajectories. Simulations were done under two regimes: (i) the action of the bath was removed from translational motion; (ii) the action of the bath was removed from both rotational and translational motion.

All simulations were performed using Venus chemical dynamics software[56] which was modified to introduce integration of Langevin equations of motion reading externally provided random forces.

Langevin Molecular Dynamics Simulations

Langevin Molecular Dynamics (LMD) simulations were performed analogously to QTB ones. The structure of equations of motion are the same as Eq 5, where now the random force is the white noise, corresponding to the classical spectral density:

$$I_{R_i} = 2m_i\gamma k_B T \tag{8}$$

and the simulations were done as previously, with the same algorithms where now a different random force is read. The same temperatures and γ values of QTB simulations were considered in LMD simulations. As previously, 500 trajectories with variable time-lengths (between 5 ps and 4 ns) as function of temperature were performed per each set of simulations. As for QTB, simulations were done under two regimes: (i) the action of the bath was removed from translational motion; (ii) the action of the bath was removed from both rotational and translational motion. The LMD dynamics was implemented in Venus as for QTB, reading an external noise.

Microcanonical Dynamics

Microcanonical simulations were done as in Ref,[45] extending the study to different internal energies: 119.9, 127.8, 131, 133, 136.6, 145.35, 154.16, 162.98 and 171.82 kcal/mol. For these energies, we run trajectories that are purely newtonian and also using the reversing momentum algorithm of Paul and Hase.[45] Briefly, the reversing momentum algorithm (here and hereafter called REV) works as follows: a newtonian simulation is performed but when the products are formed (identified in the present case by the C–H distance of 6 Å) the vibrational energy, E_{vib}, of products (here CH_3) is calculated. If $E_{vib} \geq$ ZPE (in this case the ZPE of CH_3 product) then the trajectory is considered reactive and stopped. If, otherwise, the products have not enough ZPE, the momentum of CH_3–H relative motion is reversed, corresponding to sending back the trajectory to the reactant basin. The trajectory follows

its fate and if at a certain point it reacts again, the E_{vib} of CH_3 is checked, up to fragmentation with the correct E_{vib}. More details can be found in the original paper by Paul and Hase.[45] Note that initially only the vibrational degrees of freedom are activated, which is the microcanonical counterpart of regime (ii) in QTB and LMD simulations (i.e. when the action of the bath is removed also from rotational degrees of freedom).

Also in this case, we performed 500 trajectories for each energy value and method with variable time-lengths (between 500 ps and 100 ns) in order to have almost 100 % of reactive trajectories.

Results

Canonical Lifetimes

From QTB and LMD simulations it is possible to obtain properties in the canonical ensemble and thus, if we measure the lifetime of the reactants, their canonical lifetime, $\tau(T)$, and corresponding rate constants, $k(T)$ ($k(T) = 1/\tau(T)$). In Figure 2 we show the population decay obtained at two temperatures for QTB simulations with $\gamma = 0.1 \times 10^{14}$ s^{-1}. The fitted lifetime (τ) or decay rate (k) from data of Figure 2 are also shown. Similar exponential decay is obtained for QTB and LMD simulations at different γ and temperature values.

One crucial aspect of QTB and LMD simulations is the choice of the frictional parameter, γ. $1/\gamma$ represents the characteristic time of energy exchange between the system and the thermostat and it is usually chosen higher than the lifetime of vibrational modes in order to avoid widening of peaks and bands in frequency spectra. In QTB its role is more subtle. In fact, the QTB method is prone to ZPE leakage (ZPEL) problem which results from the transfer of energy from high-frequency to low-frequency modes. Recently, Brieuc *et al.*[55] have shown that increasing the γ value reduces and even eliminates the ZPEL. A more detailed study of Mangaud et al. showed that it is possible to adapt γ on-the-fly in order to fulfill the quantum fluctuation dissipation theorem:[57] this approach is surely tempting

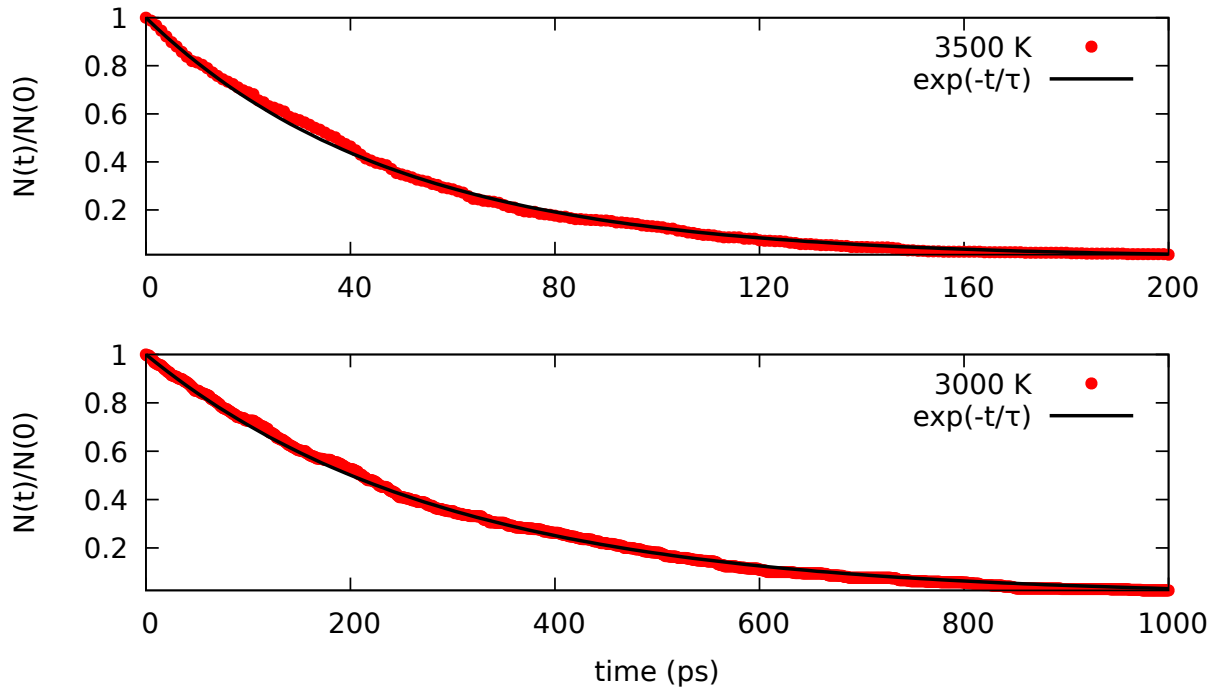

Figure 2: CH_4 population decay as obtained in QTB simulations for $\gamma = 0.1 \times 10^{14}$ s^{-1} at two different temperatures.

but needs equilibrated portion of trajectories (to calculate power spectra) so it cannot be directly used for relatively fast reactivity. However, high γ values are not possible since the bath frequency should not be in resonance with the vibrational frequencies. We have thus chosen the intermediate temperature of 4000 K to understand how τ is affected by the γ parameter. Furthermore, the coupling with rotational degrees of freedom can further increase the width, so we have performed the same tests at 4000 K also removing the bath on rotational motion. In Figure 3 we report the lifetimes for both QTB and LMD with γ in the range $0.01 - 0.5 \times 10^{14}$ s^{-1}. We notice that, for γ being in the 0.1–0.5 $\times$ 10^{14} s^{-1} range, lifetime values are relatively constant. We have thus considered this range for further analysis. Removing the bath also from rotational motion slows down the reaction, both in QTB and LMD simulations. This is quite expected since the rovibrational coupling increases the reactivity which here consists in simple dissociation of H atom. The effect of γ is the same as previously, confirming that the 0.1–0.5 $\times$ 10^{14} s^{-1} γ range provides constant lifetimes

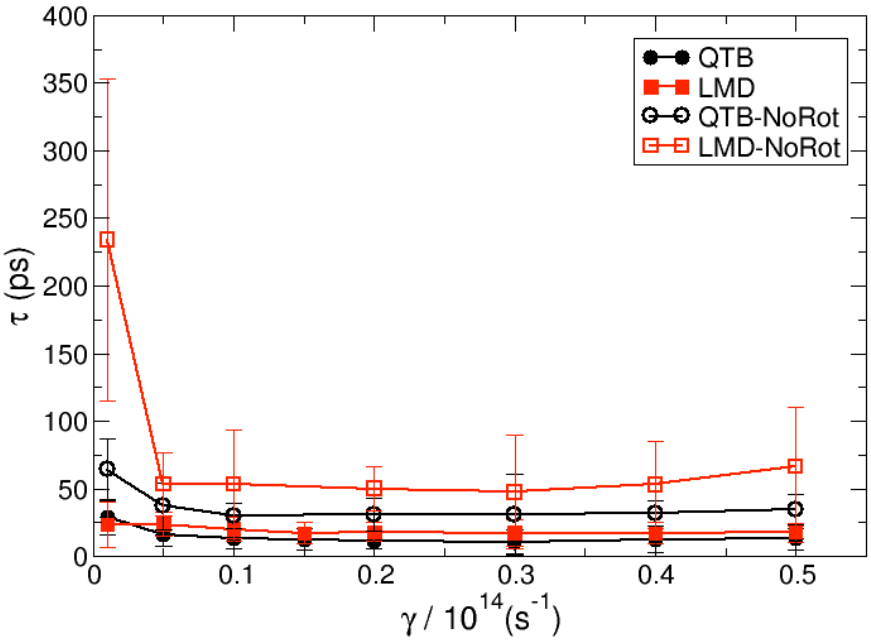

Figure 3: Canonical lifetimes for T = 4000 K as a function of γ as obtained in QTB and LMD simulations. Filled symbols are for simulations where the bath was removed only on translational degrees of freedom, open ones where it was removed also on rotational motion (labeled NoRot).

(and thus rate constants).

QTB and LMD lifetimes at different temperatures and γ values are summarized in Table 1. As we can noticed, QTB lifetimes are systematically smaller than the LMD ones at the same temperature: this is not unexpected since for the same formal temperature the classical and quantum internal energies are different (see Figure 1). This is not in contradiction with the previous microcanonical results where using REV algorithm (which considers ZPE in products) the lifetime increases with respect to classical trajectories: quantum distribution in QTB is in both reactants and products such that the effective barrier decreases when NQE are considered. On the other hand, REV algorithm controls only the ZPE of products.

Experiments and some simulations are reported in the literature.[52,58–64] However, a direct comparison with QTB and LMD results is not straightforward. In fact, experimentally, rate constants are obtained as a function of temperature and pressure: the reaction is obtained due to a shock with a gas, M, resulting in strong pressure dependence. Using thermodynamic and falloff models,[62,65] it is possible to recover a high-pressure limit rate constant which is now pressure independent and thus expressed in inverse time units. Data reported in the investigated temperature range are available in the NIST Kinetics Database[66] from experiments of Sutherland et al.[60] Corresponding lifetimes are 1712, 143, 22 and 5 ps for T = 3000, 3500, 4000 and 4500. Even if it is not clear how QTB lifetimes can be related to experimental pressure conditions, we should notice that such values are on the same order of magnitude of our results.

Activation Energies

Canonical simulations, both LMD and QTB, show temperature dependences of the rate constant which follow an Arrhenius behavior for all the γ values considered here. An example, as obtained for $\gamma = 0.2 \times 10^{14}\mathrm{s}^{-1}$, is reported in Figure 4.

We have thus fitted $k(T)$ with the well-known expression:

Table 1: Fragmentation lifetimes (in ps) as obtained in QTB and LMD (also when the bath was removed from rotation, labeled as NoRot) at different γ values.

T/K	$\gamma/10^{14}\mathrm{s}^{-1}$	QTB	QTB-NoRot	LMD	LMD-NoRot
3000	0.1	289.11	757.62	937.34	3126.37
	0.2	307.73	843.29	855.31	3189.67
	0.3	281.76	916.53	941.34	3493.33
	0.4	332.86	1146.12	999.15	3670.72
	0.5	347.77	1142.34	1171.00	4107.19
3500	0.1	48.40	111.28	93.85	272.35
	0.2	43.64	121.33	91.92	286.80
	0.3	44..55	163.54	95.63	266.16
	0.4	50.63	139.74	89.11	325.99
	0.5	54.94	167.77	104.51	389.54
4000	0.1	13.04	30.14	20.25	53.58
	0.2	11.74	31.04	18.10	50.13
	0.3	10.64	31.31	17.33	47.49
	0.4	12.13	31.85	17.08	53.00
	0.5	12.82	34.82	17.73	66.26
4500	0.1	4.45	9.81	5.97	14.44
	0.2	3.78	8.74	5.40	13.61
	0.3	3.56	9.74	4.96	13.62
	0.4	4.09	9.78	4.64	14.89
	0.5	3.61	11.61	5.19	15.04
5000	0.1	2.23	4.62	2.71	5.51
	0.2	1.77	3.80	2.08	5.01
	0.3	1.61	3.51	1.99	4.78
	0.4	1.57	3.99	1.87	4.92
	0.5	1.63	4.71	1.92	4.98
5500	0.1	1.20	2.38	1.40	2.88
	0.2	0.95	2.00	1.08	2.30
	0.3	0.86	1.89	0.99	2.18
	0.4	0.83	2.00	0.97	2.29
	0.5	0.84	2.00	1.19	2.34

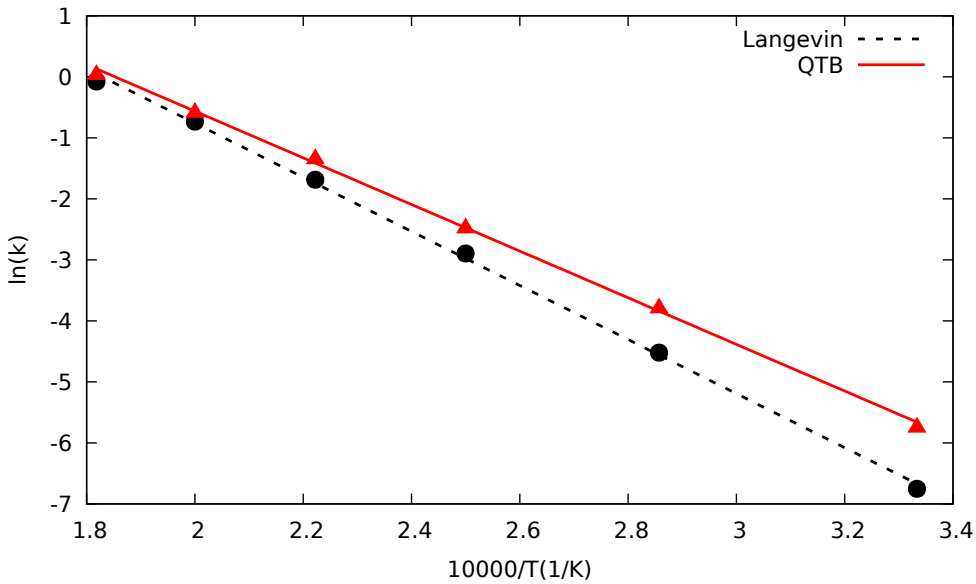

Figure 4: Arrhenius plot for $\gamma = 0.2 \times 10^{14}\mathrm{s}^{-1}$ as obtained from LMD and QTB simulation. Rate constant is in ps^{-1}.

$$k(T) = Ae^{-E_a/k_BT} \tag{9}$$

obtaining the pre-exponential factor, A, and the activation energy, E_a, for LMD and QTB simulations at different γ values. Results are reported in Table 2.

Table 2: Activation energies (in kcal/mol) and pre-exponential factors (in ps^{-1}) as obtained from QTB and LMD simulations by fitting Eq. 9. In parenthesis we report results when removing the bath also on rotational degrees of freedom.

γ	E_a^{QTB}	E_a^{LMD}	lnA^{QTB}	lnA^{LMD}
0.1	72 ± 1	85 ± 2	6.5 ± 0.1	7.6 ± 0.3
	(75 ± 1)	(92 ± 1)	(6.1 ± 0.1)	(7.5 ± 0.3)
0.2	76 ± 1	88 ± 1	7.1 ± 0.1	8.1 ± 0.2
	(78 ± 2)	(95 ± 2)	(6.5 ± 0.2)	(7.9 ± 0.3)
0.3	77 ± 1	90 ± 2	7.2 ± 0.1	8.4 ± 0.3
	(83 ± 2)	(96 ± 2)	(7.0 ± 0.2)	(8.1 ± 0.2)
0.4	79 ± 1	91 ± 2	7.6 ± 0.1	8.6 ± 0.3
	(83 ± 1)	(97 ± 2)	(7.0 ± 0.1)	(8.2 ± 0.2)
0.5	80 ± 1	93 ± 2	7.6 ± 0.1	8.7 ± 0.3
	(83 ± 1)	(99 ± 2)	(6.8 ± 0.1)	(8.3 ± 0.2)

We should note, first, that QTB activation energies are systematically lower than cor-

responding LMD ones. Furthermore, E_a increases with γ for both QTB and LMD. It is well known that activation energies obtained from Arrhenius plot of a canonical simulation are often lower than actual potential energy barriers, due to the energy fluctuations in a canonical ensemble.[67,68] Interestingly, here, the QTB values are lower than those of LMD as should be from differences in ZPE between reactants and products. In particular, from the CH_4 model employed, we will expect a difference between classical and quantum energy barrier of 10.57 kcal/mol: the differences between LMD and QTB activation energies are plot in Figure 5 at different γ values and they are very similar. They also show a smaller dependence on γ than activation energies.

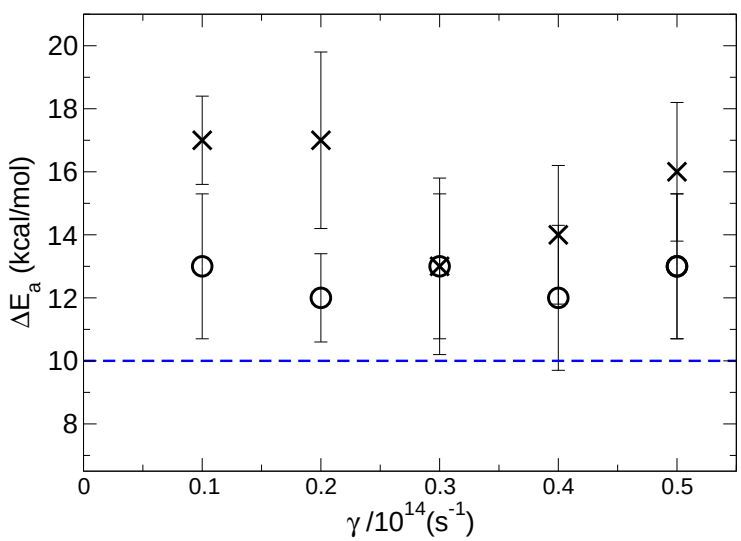

Figure 5: Differences between LMD and QTB activation energies as a function of γ. Circles correspond to simulations where the thermostat was removed only on translational motion, crosses where also rotational motion was removed. As horizontal line we report the classical-quantum difference of reaction barrier as from the potential energy surface.

We should notice that ΔE_a values obtained when removing the thermostat effect on both rotational and translational motions are systematically higher than those for which the thermostat was removed only on translational motion. In particular this reflects the larger difference between the two regimes in LMD simulations, as shown in Table 2.

Activation energies are underestimated with respect to Arrhenius fits obtained from experimental rate constants. In fact, Cobos and Troe[62] report E_a = 104.9 kcal/mol and ln(A/ps^{-1}) =10.1 and similar values are suggested for an extensive compilation of combustion chemistry kinetics, E_a = 103.8 kcal/mol and ln(A/ps^{-1}) = 8.2.[59] As we have previously remarked, E_a values are also smaller than the barrier height (D^0) which is determined by the DHS model. As discussed by Johnston and Birks years ago,[67] this can be overcome and explained using a modified-Arrhenius expression:

$$k(T) = AT^m e^{-E/k_B T} \tag{10}$$

where m is an additional parameter (negative when E_a is underestimated). One can recover the barrier high (i.e. $E \equiv D^0$) if

$$m = (E_a - D^0)/R\bar{T} \tag{11}$$

where $\bar{T}$ is the average temperature of the data set.[67] In the literature, some experimental and theoretical values were fitted with modified Arrhenius Eq. 10. Experimentally, Sutherland et al.[60] fitted high-pressure limit rate constants in the 1600-4500 K range obtaining E = 109 kcal/mol, while Kiefer and Kumaran[61] fitted low-pressure limit values finding E = 97 kcal/mol. Simulations from Marques et al.[52] with a modified DHS model provide activation energies in the 93–102 kcal/mol range as a function of the treatment of product ZPE. Our data do not show a deviation from the simple Arrhenius behavior, and fitting them with Eq. 10 we obtain large uncertainties in results and any clear behavior in activation energies (see Table S1 in the Supporting Information). We should note that also fitted values reported by Marques et al. show very large uncertainties (22 and 38 kcal/mol in activation energies).[52] Fixing m to a value of -2.4, which reduces the uncertainty on the fit, we obtain E values which are more coherent and closer to experimental and theoretical values (see Table S2 in the SI). Of course, determining m values from equation 11 (which

needs the pre-knowledge of the barrier, with here we know from the DHS model) we obtain values very close to the barrier height. Interestingly, m values determined by equation 11 are between -3.2 and -1.9 for QTB and -2.9 and -1.2 for LMD, which are close to the empirical value of -2.4.

Microcanonical Lifetimes and Barriers

Microcanonical simulations were done at fixed internal energies, and, as previously, lifetimes were obtained as function of this energy. Note that values for two energies (131 and 133 kcal/mol) correspond to results of Ref.[45] As expected, REV lifetimes are bigger than those from newtonian trajectories, because the REV algorithm has the final effect of extending the time spent by a trajectory in the reactant basin.

We can extract information on reaction barriers from evolution of rate constant as a function of internal energy. Here, the classical RRKM expression can be used since underlying trajectories follow classical equations of motions (in REV algorithm there is only a condition on when considering a trajectory done, if not fullfilled the trajectory is simply sent back to reactants). In particular, data can be fitted using the well-known RRK formula:

$$k(E) = \nu \left(\frac{E - E_0}{E} \right)^{s-1} \tag{12}$$

where E_0 is the barrier and s the number of vibrational modes of reactants. In old RRK theory, ν is an adjustable parameter with the dimension of a frequency. Here we fit the expression of Eq. 12 to get E_0 and ν, which is an effective frequency.

Other than using the pure RRK relation where the number of degrees of freedom (s) was fixed (such that $s - 1 = 8$) we also let this as a free parameter. As shown in Figure 6, this improves the rate constant fit. Resulting parameters are reported in Table 3.

The best fits are obtained when s value was added as a parameter, resulting in s values which are systematically lower than the number of degrees of freedom of the system. This is a

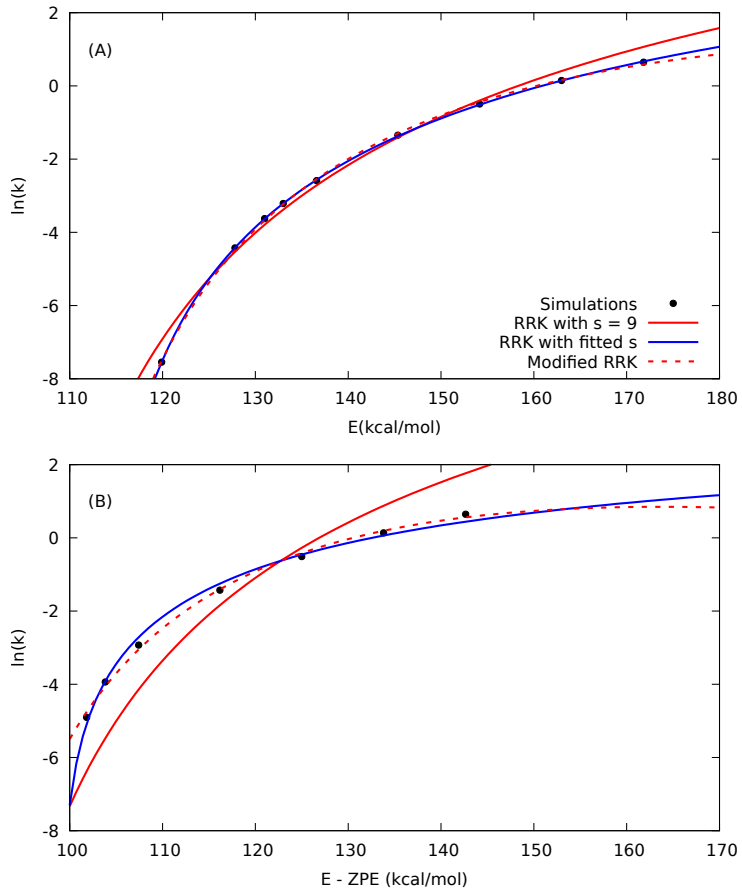

Figure 6: Rate constant (in ps^{-1}) as a function of internal energy as obtained in microcanonical simulations. (A) Newtonian simulations; (B) REV algorithm simulations.

Table 3: Energy barriers obtained and other RRK fit parameters obtained from micro-canonical simulations, both using Newton and REV dynamics. Results using Eq 12 are reported in the higher part of the table and those using Eq 13, for which s is fixed to the actual vibrational degrees of freedom, in the lower part. Δ is the difference (in kcal/mol) between Newton and REV barriers (E_0).

Simulation	E_0(kcal/mol)	ν (ps^{-1})	(s-1)	Δ
Newton	102	3904	8	–
Newton	112	338	4.9	–
REV	88	11929	8	- 14
REV	99	25	2.34	- 13
	D_0(kcal/mol)	a (ps^{-1})	b([kcal/mol]$^{-1}$)	c	Δ
Newton	107	2.19×10^6	3.44×10^{-2}	0.02	–
REV	86	4.76×10^6	5.31×10^{-2}	0.06	21

well-known issue of RRK fits and it is related to the problem of using a classical harmonic rate constant to fit a (classical) anharmonic fragmentation kinetic, as deeply discussed by Song and Hase some years ago.[69] Furthermore, one should consider the energy dependent behavior of the threshold in the case of unimolecular decomposition. The same authors proposed a modified expression for the RRK rate constant, where now frequency and threshold energy are energy dependent:

$$k(E) = \nu(E) \left[\frac{E - E_0(E)}{E} \right]^{s-1} \tag{13}$$

The energy dependence of the threshold can be expressed as:

$$E_0(E) = D_0 - cE_\infty \tag{14}$$

where D_0 is the dissociation energy and $E_\infty = E - D_0$.

The $\nu(E)$ takes into account (i) the energy dependence in the anharmonic correction ratio between sum and density of states and (ii) the tightens in variational transition state vibrational frequencies with increasing E. A simple expression was proposed by Song and Hase:[69]

$$\nu(E) = a f_{anh}(E) \tag{15}$$

For $f_{anh}(E)$ different forms are possible, Song and Hase have found that for CH_4 dissociation the best way is using

$$f_{anh}(E) = \frac{\exp\left[b^\dagger (E - E_0)\right]}{\exp\left(bE\right)\left[1 + \frac{bE}{s}\right]} \tag{16}$$

where b is for reactants and $b^\dagger$ for transition state.

The modified RRK expression of Eq. 13 depends now only on four fitted parameters, a, b, $b^\dagger$ and c if one knows D_0. The fitted values for newtonian dynamics are reported in Table 3.

As in the original work,[69] $b^\dagger = 0$ permits a good fit.

When fixing D_0 to the known classical threshold, a, b and c values are similar to the one reported for the same reaction with a slightly different model.[69] When letting D_0 varying as a free parameter, it slightly changes but more importantly other parameters change largely, in particular a and c.

In the case of REV simulations, it was not possible to provide a fit with a physical meaning when fixing D_0 to the known value. Considering D_0 as an additional fitted quantity (and the ZPE of reactants), we have two slightly similar values (about 86 kcal/mol) for both $b^\dagger = 0$ and $b^\dagger \neq 0$. The threshold is now 20 kcal/mol lower than the classical one and 10 kcal/mol too low than when adding ZPE in reactant and products. One reason can reside in the arbitrary modification in dynamics when doing REV simulations, resulting in irregular behavior of unimolecular fragmentation kinetics. Another possible reason is that the modified RRK approach is not appropriate to model unimolecular dissociation with REV method. Finally, other anharmonicity functions exist, in particular based on works of Troe,[70,71] and it would be interesting to explore them deeper in details in works focusing on microcanonical theories, which is, however, beyond the aim of the present paper.

Concluding, microcanonical simulations, in particular using standard RRK expression, can recover the quantum vs classical energy difference. Barrier values are similar to what expected from the analytical potential in particular if also the number of degrees of freedom is considered as a fit variable.

Classical vs Quantum Rate Constants

Direct comparison between rate constants obtained from LMD and QTB and Newtonian and REV simulations cannot be done because the former lifetimes (and rate constant) are canonical while the latter microcanonical. From Arrhenius and RRK fits it was possible to extrapolate activation and threshold energies which can be compared. In particular, as we have discussed, simulations report that barriers from QTB and REV are lower than those

from LMD and Newtonian simulations (as expected) and the differences are similar to what expected from the reaction energy barrier.

A more detailed comparison can be done by calculating the canonical rate constant, $k(T)$, from the micro-canonical one, $k(E)$, using the well known relationship:

$$k(T) = \frac{1}{Q(T)} \int k(E)\rho(E)e^{-\beta E} dE \tag{17}$$

where $Q(T)$ is the partition function (here only vibrational motion was considered to be coherent with microcanonical initial conditions) and $\rho(E)$ the density of states.

In Figure 7A we compare Newtonian microcanonical simulations with LMD ones for different γ values and where the thermostat was removed from both translational and rotational motions (labeled NoRot) and only from translational one. Rate constants using integrated Newtonian microcanonical values are very close to LMD-NoRot ones. In panel B of the same Figure 7 we report REV integrated rate constants compared to QTB results. In this case, REV rate constants are systematically lower than QTB values and in any case closer to QTB-NoRot ones. As we discussed previously, the REV dynamics is biased and it is not clear how (and if) kinetic theory is applicable.

Overall the comparison shows that QTB and REV simulations provide similar results and that QTB is a promising way of using direct dynamics simulations to estimate unimolecular rate constants.

Conclusions

In the present work we have investigated the possibility of using the Quantum Thermal Bath method to include nuclear quantum effects in unimolecular dissociation trajectory simulations. In particular, we were interested in the problem of rate constant modification due to difference in products and reactants vibrational zero-point energies. At this aim we have considered the fragmentation of a model CH_4 for which microcanonical algorithms were

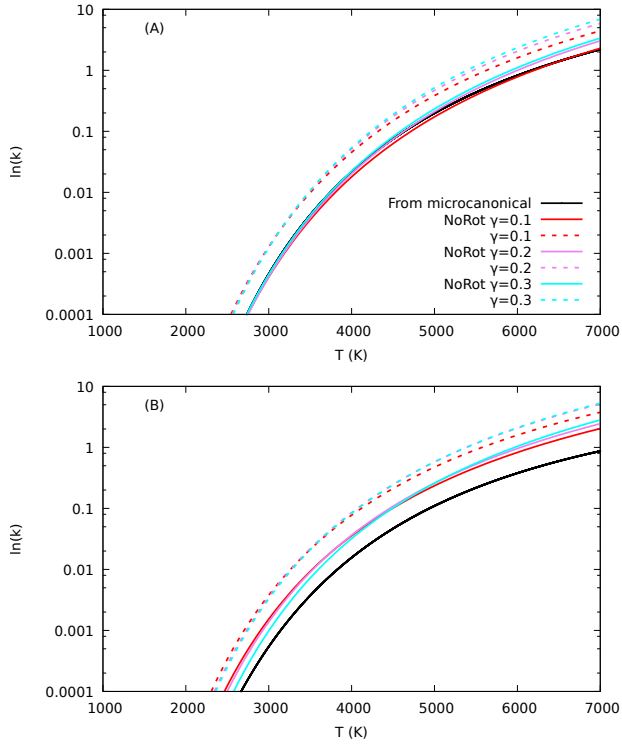

Figure 7: Rate constant (in ps^{-1}) as a function of temperature as obtained by canonical simulations at different γ values and from integrated microcanonical rate constants using Eq. 17. Panel A: newtonian and LMD simulation results; panel B: REV and QTB simulation results. Different γ values are shown in both LMD and QTB simulations. NoRot means that the thermostat (LMD or QTB) is removed also from rotational degrees of freedom.

developed in order to take into account this specific problem. QTB was shown to being able to catch the key feature of the difference between classical and quantum kinetics, i.e. a difference in activation energy of about 10 kcal/mol, with values similar to modified microcanonical algorithm. In this last microcanonical method, it is necessary to know in advance the ZPE of both reactants and products to obtain the correct behavior. The advantage of QTB is that results are directly obtained from simulations without any pre-knowledge of the ZPE, because the algorithm is tailored to fulfill at best the quantum fluctuation dissipation relationship.

Here we have considered a 3000–5500 K temperature range, where the difference between classical and quantum vibrational energy is between 18% and 6%. However, this difference and, more importantly, the different noise structure in Langevin-type equations, were enough to obtain differences in activation energy, reflecting the classical/quantum reaction barrier difference. Decreasing temperature range will need exponentially longer simulations to have converged lifetimes. Likely, at lower temperatures non-Arrhenius behavior will appear, which will be interested to be studied with QTB using a more reactive system. Furthermore, it will be surely interesting to study unimolecular reactions coupled with proton transfer. This is now possible since QTB was tested on proton transfer[42–44] and unimolecular dissociation (this work) separately.

Note that QTB has the computational advantage of being comparable in simulation time with a standard newtonian dynamics, thus making this approach promising for studying direct reaction dynamics of more complex molecular systems. One critical parameter of QTB is the friction value which was subject to careful analysis in the present work. Surely more studies are needed to find the best parameters for simulations of isolated molecules and ions with organic and biological interest. Our research is going in that direction.

Associated Content

In the Supporting Information we report the details of the model employed for $CH_4 \rightarrow \cdot CH_3 + \cdot H$ reaction. We also report fits of our canonical rate constants with modified Arrhenius Eq. 10.

Acknowledgement

We thank ANR DynBioReact (Grant No. ANR-14-CE06-0029-01) and CNRS program INFINITI (project ASTROCOL) for support. We also thank William L. Hase for useful discussions and for providing us the modified version of Venus and input for microcanonical simulations.

References

(1) Baer, T.; Hase, W. L. *Unimolecular reaction dynamics: theory and experiments*; Oxford University Press, New York, 1996.

(2) Bunker, D. L. Monte Carlo Calculation of Triatomic Dissociation Rates. I. N_2O. *J. Chem. Phys.* **1962**, *37*, 393–403.

(3) Forst, W. *Theory of unimolecular reactions*; Academic Press, New York, 1973.

(4) Wardlaw, D. M.; Marcus, R. A. On the statistical theory of unimolecular processes. *Adv. Chem. Phys.* **1988**, *70*, 231–263.

(5) Klots, C. E. Reformulation of the quasi-equilibrium theory of ionic fragmentation. *J. Phys. Chem.* **1971**, *75*, 1526–1532.

(6) Klots, C. E. Quasi-equilibrium theory of ionic fragmentation: further considerations. *Z. Naturforsch.* **1972**, *27a*, 553–561.

(7) Klots, C. E. Thermochemical and kinetic information from metastable decompositions of ions. *J. Chem. Phys.* **1973**, *58*, 5364.

(8) Lourderaj, U.; McAfee, J. L.; Hase, W. L. Potential Energy Surface and Unimolecular Dynamics of Stretched n-Butane. *J. Chem. Phys.* **2008**, *129*, 094701.

(9) Yang, L.; Sun, R.; Hase, W. L. Use of Direct Dynamics Simulations to Determine Unimolecular Reaction Paths and Arrhenius Parameters for Large Molecules. *J. Chem. Theory Comput.* **2012**, *7*, 3478–3483.

(10) Ma, X.; Paul, A. K.; Hase, W. L. Chemical Dynamics Simulations of Benzene Dimer Dissociation. *J. Phys. Chem. A* **2015**, *119*, 6631–6640.

(11) Kolakkandy, S.; Paul, A. K.; Pratihar, S.; Kohale, S. C.; Barnes, G. L.; Wang, H.; Hase, W. L. Energy and Temperature Dependent Dissociation of the Na^+(benzene)$_{1,2}$ Clusters. Importance of Anharmonicity. *J. Chem. Phys.* **2015**, *142*, 044306.

(12) Song, K.; Spezia, R. *Theoretical Mass Spectrometry*; De Gruyter, Berlin, 2018.

(13) Spezia, R.; Salpin, J.-Y.; Gaigeot, M.-P.; Hase, W.; Song, K. Protonated Urea Collision-Induced Dissociation. Comparison of Experiments and Chemical Dynamics Simulations. *J. Phys. Chem. A* **2009**, *113*, 13853–13862.

(14) Spezia, R.; Cimas, A.; Gaigeot, M.-P.; Salpin, J.-Y.; Song, K.; Hase, W. Collision Induced Dissociation of Doubly-charged Ions: Coulomb Explosion vs Neutral Loss in $[Ca(urea)]^{2+}$ Gas Phase Unimolecular Reactivity via Chemical Dynamics Simulations. *Phys. Chem. Chem. Phys.* **2012**, *14*, 11724–11736.

(15) Martin-Somer, A.; Yanez, M.; Gaigeot, M.-P.; Spezia, R. Unimolecular Fragmentation Induced By Low Energy Collision: Statistically Or Dynamically Driven? *J. Phys. Chem. A* **2014**, *118*, 10882–10893.

(16) Spezia, R.; Martin-Somer, A.; Macaluso, V.; Homayoon, Z.; Pratihar, S.; Hase, W. L. Unimolecular Dissociation of Peptides: Statistical vs Non-Statistical Fragmentation Mechanisms and Time Scales. *Faraday Discuss.* **2016**, *195*, 599–618.

(17) Martin-Somer, A.; Martens, J.; Grzetic, J.; Hase, W. L.; Oomens, J.; Spezia, R. Unimolecular fragmentation of deprotonated diproline $[Pro_2\text{-}H]^-$ studied by chemical dynamics simulations and IRMPD spectroscopy. *J. Phys. Chem. A* **2018**, *122*, 2612–2625.

(18) Homayoon, Z.; Pratihar, S.; Dratz, E.; Snider, R.; Spezia, R.; Barnes, G.; Macaluso, V.; Martin-Somer, A.; Hase, W. L. Model Simulations of the Thermal Dissociation of the $TIK(H^+)_2$ tripeptide. Mechanisms and Kinetic Parameters. *J. Phys. Chem. A* **2016**, *120*, 8211–8227.

(19) Spezia, R.; Martens, J.; Oomens, J.; Song, K. Collision-induced dissociation pathways of protonated Gly_2NH_2 and Gly_3NH_2 in the short time-scale limit by chemical dynamics and ion spectroscopy. *Int. J. Mass Spectrom.* **2015**, *388*, 40–52.

(20) Spezia, R.; Lee, S. B.; Cho, A.; Song, K. Collision Induced Dissociation Mechanisms of Protonated Penta- and Octa-Glycine as Revealed by Chemical Dynamics Simulations. *Int. J. Mass Spectrom.* **2015**, *392*, 125–138.

(21) Ortiz, D.; Salpin, J.-Y.; Song, K.; Spezia, R. Galactose 6-sulfate collision induced dissociation using QM+MM chemical dynamics simulations and ESI-MS/MS experiments. *Int. J. Mass Spectrom.* **2014**, *358*, 25–35.

(22) Rossich Molina, E.; Eizaguirre, A.; Haldys, V.; Urban, D.; Doisneau, G.; Bourdreux, Y.; J.-M.Beau,; Salpin, J.-Y.; R.Spezia, Characterization of protonated model disaccharides from tandem mass spectrometry and chemical dynamics simulations. *ChemPhysChem* **2017**, *18*, 2812–2823.

(23) Craig, I. R.; Manolopoulos, D. E. Quantum statistics and classical mechanics: Real time correlation functions from ring polymer molecular dynamics. *J. Chem. Phys.* **2004**, *121*, 3368.

(24) Cao, J.; Voth, G. A. The formulation of quantum statistical mechanics based on the Feynman path centroid density. II. Dynamical properties. *J. Chem. Phys.* **1994**, *100*, 5106–5117.

(25) Habershon, S.; Manolopoulos, D. E. Zero point energy leakage in condensed phase dynamics: An assessment of quantum simulation methods for liquid water. *J. Chem. Phys.* **2009**, *131*, 244518.

(26) Perez de Tudela, R.; Aoiz, F. J.; Suleimanov, Y. V.; Manolopoulos, D. E. Chemical reaction rates from ring polymer molecular dynamics: Zero point energy conservation in Mu + H_2 to MuH + H. *J. Phys. Chem. Lett.* **2012**, *3*, 493–497.

(27) Feynman, R. P.; Hibbs, A. R. *Quantum mechanics and path integrals*; McGraw-Hill, New York, 1965.

(28) Feynman, R. P. *Statistical mechanics*; Addison-Wesley, Reading, MA, 1972.

(29) Berne, B. J.; Thirumalai, D. On the Simulation of Quantum Systems: Path Integral Methods. *Ann. Rev. Phys. Chem.* **1986**, *37*, 401–424.

(30) Perez, A.; Tuckerman, M. E.; Muser, M. H. A comparative study of the centroid and ring-polymer molecular dynamics methods for approximating quantum time correlation functions from path integrals. *J. Chem. Phys.* **2009**, *130*, 184105.

(31) Kay, K. G. Semiclassical Initial Value Treatments of Atoms and Molecules. *Annu. Rev. Phys. Chem.* **2005**, *56*, 255–280.

(32) Buchholz, M.; Fallacara, E.; Gottwald, F.; Ceotto, M.; Grossmann, F.; Ivanov, S. D. Herman-Kluk propagator is free from zero-point energy leakage. *Chem. Phys.* **2018**, *515*, 231–235.

(33) Herman, M. F.; Kluk, E. A semiclassical justification for the use of non-spreading wavepackets in dynamics calculations. *Chem. Phys.* **1984**, *91*, 27–34.

(34) Bowman, J. M.; Gazdy, B.; Sun, Q. A method to constrain vibrational energy in quasiclassical trajectory calculations. *J. Chem. Phys.* **1989**, *91*, 2859.

(35) Czakó, G.; Kaledin, A. L.; Bowman, J. M. A practical method to avoid zero-point leak in molecular dynamics calculations: Application to the water dimer. *J. Chem. Phys.* **2010**, *132*, 164103.

(36) Lim, K. F.; McCormack, D. A. The conservation of quantum zero-point energies in classical trajectory simulations. *J. Chem. Phys.* **1995**, *102*, 1705.

(37) McCormack, D. A.; Lim, K. F. The zero-point energy problem in classical trajectory simulations at dissociation threshold. *J. Chem. Phys.* **1997**, *106*, 572.

(38) Dammak, H.; Chalopin, Y.; Laroche, M.; Hayoun, M.; Greffet, J.-J. Quantum Thermal Bath for Molecular Dynamics Simulation. *Phys. Rev. Lett.* **2009**, *103*, 190601.

(39) Dammak, H.; Antoshchenkova, E.; Hayoun, M.; Finocchi, F. Isotope effects in lithium hydride and lithium deuteride crystals by molecular dynamics simulations. *J. Phys. Cond. Matt.* **2012**, *24*, 435402.

(40) Calvo, F.; Van-Oanh, N.; Parneix, P.; Falvo, C. Vibrational spectra of polyatomic molecules assisted by quantum thermal baths. *Phys. Chem. Chem. Phys.* **2012**, *14*, 10503.

(41) Savin, A. V.; Kosevich, Y. A.; Cantarero, A. Semiquantum molecular dynamics simulation of thermal properties and heat transport in low-dimensional nanostructures. *Phys. Rev. B* **2012**, *86*, 064305.

(42) Basire, M.; Borgis, D.; Vuilleumier, R. Computing Wigner distributions and time correlation functions using the quantum thermal bath method: application to proton transfer spectroscopy. *Phys. Chem. Chem. Phys.* **2013**, *15*, 12591.

(43) Bronstein, Y.; Depondt, P.; Finocchi, F.; Saitta, A. M. Quantum-driven phase transition in ice described via an efficient Langevin approach. *Phys. Rev. B* **2014**, *89*, 214101.

(44) Bronstein, Y.; Depondt, P.; Finocchi, F. Thermal and nuclear quantum effects in the hydrogen bond dynamical symmetrization phase transition of -AlOOH. *Eur. J. Mineral.* **2017**, *29*, 385–395.

(45) Paul, A.; Hase, W. L. Zero-Point Energy Constraint for Unimolecular Dissociation Reactions. Giving Trajectories Multiple Chances To Dissociate Correctly. *J. Phys. Chem. A* **2016**, *120*, 372–378.

(46) Miller, W. H.; Hase, W. L.; Darling, C. L. A simple model for correcting the zero point energy problem in classical trajectory simulations of polyatomic molecules. *J. Chem. Phys.* **1989**, *91*, 2863.

(47) Duchovic, R. J.; Hase, W. L.; Schlegel, H. B. Analytic Function for the H + CH_3 = CH_4 Potential Energy Surface. *J. Phys. Chem.* **1984**, *88*, 1339.

(48) Hase, W. L.; Mondro, S. L.; Duchovic, R. J.; Hirst, D. M. Thermal Rate Constant for H + CH_3 $\rightarrow$ CH_4 Recombination. 3. Comparison of Experiment and Canonical Variational Transition State Theory. *J. Am. Chem. Soc.* **1987**, *109*, 2916–2922.

(49) Hu, X.; Hase, W. L. Modification of the DHS Analytic Potential Energy Function for H + CH_3 $\rightarrow$ CH_4. Comparison of CVTST, Trajectory and Experimental Association Rate Constants. *J. Chem. Phys.* **1991**, *95*, 8073–8082.

(50) Warmbier, R.; Schneider, P.; Sharma, A. R.; Braams, B. J.; Bowman, J. M.; Hauschildt, P. H. Ab Initio Modeling of Molecular IR Spectra of Astrophysical Interest: Application to CH_4. *Astron. Astrophys.* **2009**, *495*, 655–661.

(51) Conte, R.; Houston, P. L.; Bowman, J. M. Trajectory and Model Studies of Collisions of Highly Excited Methane with Water Using and ab Initio Potential. *J. Phys. Chem. A* **2015**, *119*, 12304–12317.

(52) Marques, J. M. C.; Martinez-Nunez, E.; Fernandez-Ramos, A.; ; Vazquez, S. A. Trajectory Dynamics Study of the Ar + CH_4 Dissociation Reaction at High Temperatures: the Importance of Zero-Point-Energy Effects. *J. Phys. Chem. A* **2005**, *109*, 5415–5423.

(53) Callen, H. B.; Welton, T. A. Irreversibility and Generalized Noise. *Phys. Rev.* **1951**, *83*, 34.

(54) Chalopin, Y.; Dammak, H.; Laroche, M.; Hayoun, M.; Greffet, J. J. Radiative heat transfer from a black body to dielectric nanoparticles. *Phys. Rev. B* **2011**, *84*, 224301.

(55) Brieuc, F.; Bronstein, Y.; Dammak, H.; Depondt, P.; Finocchi, F.; Hayoun, M. Zero-Point Energy Leakage in Quantum Thermal Bath Molecular Dynamics Simulations. *J. Chem. Theory Comput.* **2016**, *12*, 5688–5697.

(56) Hase, W. L.; Duchovic, R. J.; Hu, X.; Komornicki, A.; Lim, K. F.; Lu, D.-H.; Peslherbe, G. H.; Swamy, K. N.; Linde, S. R. V.; Varandas, A. et al. VENUS. A General Chemical Dynamics Computer Program. *QCPE Bull.* **1996**, *16*, 671.

(57) Mangaud, E.; Huppert, S.; Pl, T.; Depondt, P.; Bonella, S.; Finocchi, F. The FluctuationDissipation Theorem as a Diagnosis and Cure for Zero-Point Energy Leakage in Quantum Thermal Bath Simulations. *J. Chem. Theory Comput.* **2019**, *15*, 2863–2880.

(58) Chen, C.-J.; Back, M. H.; Back, R. A. The Thermal Decomposition of Methane. I. Kinetics of the Primary Decomposition to C_2H_6 + H_2; Rate Constant for the Homogeneous Unimolecular Dissociation of Methane and its Pressure Dependence. *Can. J. Chem.* **1975**, *53*, 3580–3590.

(59) Tsang, W.; Hampson, R. F. Chemical Kinetic Data Base for Combustion Chemistry. Part I. Methane and Related Compounds. *Journal of Physical and Chemical Reference Data* **1986**, *15*, 1087–1279.

(60) Sutherland, J. W.; Su, M. C.; Michel, J. V. Rate Constants for H + CH_4, CH_3 + H_2, and CH_4 Dissociation at High Temperature. *Int. J. Chem. Kin.* **2001**, *33*, 669–684.

(61) Kiefer, J. H.; Kumaran, S. S. Rate of CH_4 Dissociation over 2800-4300 K: The Low-Pressure-Limit Rate Constant. *J. Phys. Chem.* **1993**, *97*, 414–420.

(62) Cobos, C. J.; Troe, J. CH_4 + M $\Leftrightarrow$ CH_3 + H + M: II. Evaluation of Experiments up to 5000 K and Temperature Dependence of $\langle \Delta E \rangle$. *Z. Phys. Chem.* **1992**, *176*, 161–171.

(63) Jasper, A. W.; Miller, J. A. Collisional Energy Transfer in Unimolecular Reactions:

Direct Classical Trajectories for $CH_4 \Leftrightarrow CH_3 + H$ in Helium. *J. Phys. Chem. A* **2009**, *113*, 5612–5619.

(64) Jasper, A. W.; Miller, J. A. Theoretical Unimolecular Kinetics for $CH_4 + M \Leftrightarrow CH_3 + H + M$ in Eight Baths, M = He, Ne, Ar, Kr, H_2, N_2, CO, and CH_4. *J. Phys. Chem. A* **2011**, *115*, 6438–6455.

(65) Troe, J.; Ushakov, V. G. The dissociation/recombination reaction CH_4 (+ M) $\Leftrightarrow CH_3$ + H (+ M): A case study for unimolecular rate theory. *Z. Phys. Chem.* **1992**, *176*, 161–171.

(66) Manion, J. A.; Huie, R. E.; Levin, R. D.; Burgess Jr., D. R.; Orkin, V. L.; Tsang, W.; McGivern, W. S.; Hudgens, J. W.; Knyazev, V. D.; Atkinson, D. B. et al. 2015.

(67) Johnston, H.; Birks, J. Activation Energies for the Dissociation of Diatomic Molecules Are Less than the Bond Dissociation Energies. *Acc. Chem. Res.* **1972**, *5*, 327–335.

(68) Truhlar, D. Interpretation of the Activation Energy. *J. Chem. Edu.* **1978**, *55*, 309–311.

(69) Song, K.; Hase, W. L. Fitting classical microcanonical unimolecular rate constants to a modified RRK expression: Anharmonic and variational effects. *J. Chem. Phys.* **1999**, *110*, 6198–6207.

(70) Troe, J. Specific rate constants k(E,J) for unimolecular bond fissions. *J. Chem. Phys.* **1983**, *79*, 6017.

(71) Troe, J. Simplified models for anharmonic numbers and densities of vibrational states. I. Application to NO_2 and H_3^+. *Chem. Phys.* **1995**, *190*, 381–392.
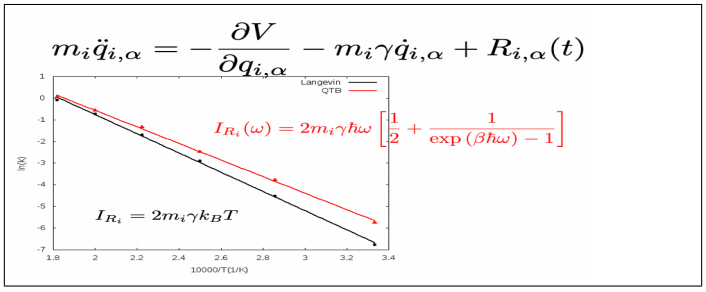
Graphical TOC Entry